

# N-dimensional maximum-entropy tomography via particle sampling

Austin Hoover\*

Oak Ridge National Laboratory, Oak Ridge, Tennessee 37830, USA

(Dated: September 27, 2024)

This paper proposes an alternative implementation of the MENT algorithm, an exact maximum-entropy algorithm used to infer a phase space distribution from its projections. A key step in the MENT algorithm is to compute the distribution's projections via numerical integration. In this approach, the run time scales quickly with the phase space dimension and measurement resolution. The proposed MENT implementation computes the projections via particle sampling, rather than numerical integration, eliminating the dependence on the measurement resolution. Furthermore, with the appropriate sampling algorithm, the particle-based approach scales to  $N$ -dimensions without computer memory limitations. Using synthetic data, we demonstrate MENT convergence in four dimensions using a grid-based sampling method and in six dimensions using Markov Chain Monte Carlo (MCMC) sampling.

## I. INTRODUCTION

Classical particle ensembles evolve in a two-dimensional, four-dimensional, or six-dimensional phase space. *Phase space tomography* is a family of methods to infer the phase space distribution from its projections onto lower-dimensional planes. While two-dimensional tomography is an established technique [1], higher-dimensional tomography introduces several challenges. The first challenge is to fit the data: searching the space of high-dimensional distribution functions is not straightforward [2, 3]. The second challenge is to regularize the solution and quantify the reconstruction uncertainty: increasing the phase space dimension can generate an ill-posed inverse problem [4].

Our approach to such inverse problems is the method of maximum relative entropy (ME): we update a prior probability distribution over the phase space coordinates to a posterior by maximizing the entropy of the posterior relative to the prior, subject to a set of constraints [5, 6]. While theoretically appealing, ME is a difficult constrained optimization problem. The MENT algorithm [7] is unique in that it generates an *exact* constrained maximum upon convergence. MENT is valid for any phase space dimension and is compatible with arbitrary phase space transformations. However, the run time scales quickly with the phase space dimension and the measurement resolution, as each iteration requires simulating the projections via numerical integration. At the time of writing, there have been two published four-dimensional MENT reconstructions using relatively few projections [8, 9]; no higher-dimensional MENT reconstructions have been reported.

This paper proposes an implementation of the MENT algorithm that uses particle sampling, rather than numerical integration, to simulate the projections. This approach eliminates the dependence of the run time on the measurement resolution. Furthermore, with the appropriate sampling algorithm, the particle-based approach

scales to  $N$ -dimensional phase space without computer memory limitations.

We begin by reviewing the motivation behind the maximum entropy method in Section II and the MENT algorithm in Section III. Section IV then introduces the particle-based MENT implementation, and section V demonstrates convergence in four- and six-dimensional toy problems. Section VI concludes.

## II. BACKGROUND

Our task is to infer a probability distribution  $\rho(\mathbf{x})$ , defined over phase space coordinates  $\mathbf{x} \in \mathbb{R}^N$ , from its projections onto a set of  $M$ -dimensional planes. We assume the  $k$ th of  $K$  measurements occurs after a transformation  $\mathcal{M}_k : \mathbb{R}^N \rightarrow \mathbb{R}^M$ ; we measure the projection of the transformed coordinates

$$\mathbf{u}_k = \mathcal{M}_k(\mathbf{x}) \quad (1)$$

onto an axis  $\mathbf{u}_{k\parallel} \in \mathbb{R}^M$ . The projection is the integral of  $\rho(\mathbf{x})$  over the plane  $\mathbf{u}_{k\perp} \in \mathbb{R}^{N-M}$ , which is orthogonal to  $\mathbf{u}_{k\parallel}$ . (In conventional tomography,  $N = 2$  and  $M = 1$ .) We seek a distribution  $\tilde{\rho}(\mathbf{x})$  such that

$$G_k[\tilde{\rho}(\mathbf{x})] = g_k(\mathbf{u}_{k\parallel}) - \tilde{g}_k(\mathbf{u}_{k\parallel}) = 0, \quad (2)$$

where

$$g_k(\mathbf{u}_{k\parallel}) = \int \rho(\mathbf{x}(\mathbf{u}_k)) d\mathbf{u}_{k\perp} \quad (3)$$

are the *measured* projections and

$$\tilde{g}_k(\mathbf{u}_{k\parallel}) = \int \tilde{\rho}(\mathbf{x}(\mathbf{u}_k)) d\mathbf{u}_{k\perp} \quad (4)$$

are the *simulated* projections. Going forward, we will let  $\rho(\mathbf{x})$  refer to the proposed distribution rather than the (unknown) true distribution.

There are an infinite number of distributions compatible with the constraints in Eq. (2). The only way to break the degeneracy is to incorporate prior information; such

\* hooveram@ornl.gov

information provides additional constraints. We thus define a “prior” distribution  $\rho_*(\mathbf{x})$ , representing our confidence that a particle would land near  $\mathbf{x}$  if sampled from the true distribution. We then update the prior to a “posterior”  $\rho(\mathbf{x})$  by enforcing consistency with the constraints. We do this by ranking candidate distributions via a functional  $S[\rho(\mathbf{x}), \rho_*(\mathbf{x})]$ , which we call the entropy, and selecting the highest ranked distribution.

The method of maximum relative entropy (ME) stems from the requirement that the prior should change as little as possible to fit the data. This requirement is enforced via two axioms, which we paraphrase from [6]: (i) *Subset independence*: Probabilities conditioned on one domain should not be affected by information about a different, non-overlapping domain. Consequently, non-overlapping domains must contribute additively to the entropy. (ii) *Subsystem independence*: If we initially assume two variables are unrelated, and if we receive information about each variable separately, then we should not infer any relationship between the variables on the basis of this information. In other words, if we measure the marginal distributions  $\{\rho(\mathbf{v}), \rho(\mathbf{w})\}$ , and if the prior does not encode any relationship between  $\mathbf{v}$  and  $\mathbf{w}$ , then the posterior should be the product of the marginals:  $\rho(\mathbf{v}, \mathbf{w}) = \rho(\mathbf{v})\rho(\mathbf{w})$ . The entropy functional is uniquely determined from these axioms:

$$S[\rho(\mathbf{x}), \rho_*(\mathbf{x})] = - \int \rho(\mathbf{x}) \log \left( \frac{\rho(\mathbf{x})}{\rho_*(\mathbf{x})} \right) d\mathbf{x}. \quad (5)$$

The entropy is zero if and only if  $\rho(\mathbf{x}) = \rho_*(\mathbf{x})$ ; otherwise it is negative. Bayesian updating is a specific case of ME in which there are an infinite number of constraints [6].

The form of the posterior distribution can be derived from the functional

$$\Psi = S[\rho(\mathbf{x}), \rho_*(\mathbf{x})] + \sum_k \int \lambda_k(\mathbf{u}_{k\parallel}) G_k[\rho(\mathbf{x})] d\mathbf{u}_{k\parallel}, \quad (6)$$

where  $\lambda_k(\mathbf{u}_{k\parallel})$  are Lagrange multiplier functions [10]. Enforcing zero variation of  $\Psi$  with respect to  $\rho(\mathbf{x})$  and  $\lambda_k(\mathbf{u}_{k\parallel})$  gives

$$\begin{aligned} \rho(\mathbf{x}) &= \rho_*(\mathbf{x}) \prod_k \exp(\lambda_k(\mathbf{u}_{k\parallel}(\mathbf{x}))) \\ &= \rho_*(\mathbf{x}) \prod_k h_k(\mathbf{u}_{k\parallel}(\mathbf{x})). \end{aligned} \quad (7)$$

where we have defined the “component” functions  $h_k(\mathbf{u}_k) = \exp(\lambda_k(\mathbf{u}_k))$ . This solution does not assume

the transformations  $\mathcal{M}_k$  are linear, nor that they are symplectic.

If we find functions  $h_k(\mathbf{u}_{k\parallel})$  such that the distribution in (7) generates the measured projections, then we have found the exact constrained entropy maximum—no regularization parameter is needed. We must solve the system of integral equations that results from substituting Eq. (7) into Eq. (2):

$$g_k(\mathbf{u}_{k\parallel}) = \int \rho_*(\mathbf{x}(\mathbf{u}_k)) \prod_j h_j(\mathbf{u}_{j\parallel}(\mathbf{u}_k)) d\mathbf{u}_{k\perp}. \quad (8)$$

We typically evaluate the  $g_k(\mathbf{u}_{k\parallel})$  at a finite number of points and define continuous functions by interpolation; in this case, the component functions are defined by a finite set of positive numbers  $\theta$  (the function values at the evaluation points). We are left with an unconstrained optimization over  $\theta$ .

### III. MENT

The MENT algorithm [7] solves for the component functions using a Gauss-Seidel relaxation method. Note that  $h_k(\mathbf{u}_{k\parallel})$  is a function of  $\mathbf{u}_{k\parallel}$ , which is orthogonal to the integration axis  $\mathbf{u}_{k\perp}$ ; thus,  $h_k$  can be factored out of the integral in Eq. (8). Rearranging gives a set of consistency conditions:

$$h_k(\mathbf{u}_{k\parallel}) = \frac{g_k(\mathbf{u}_{k\parallel})}{\int \rho_*(\mathbf{x}(\mathbf{u}_k)) \prod_{j \neq k} h_j(\mathbf{u}_{j\parallel}(\mathbf{u}_k)) d\mathbf{u}_{k\perp}}. \quad (9)$$

MENT begins by initializing the distribution to the prior within the measurement boundaries:

$$h_k^{(0)}(\mathbf{u}_{k\parallel}) = \begin{cases} 1, & \text{if } g_k(\mathbf{u}_{k\parallel}) > 0 \\ 0, & \text{otherwise} \end{cases} \quad (10)$$

where the superscript represents the iteration number, so that, initially,

$$\rho^{(0)}(\mathbf{x}) = \rho_*(\mathbf{x}) \Theta \left[ \prod_k g_k(\mathbf{u}_{k\parallel}(\mathbf{x})) \right], \quad (11)$$

where  $\Theta$  is the Heaviside step function. Next, for each measurement index  $k$ , we set the  $k$ th component function  $h_k$  equal to the right-hand side of Eq. (9), then immediately uses the new  $h_k$  to update  $h_{k+1}$ . In other words, for each iteration  $i$  and measurement index  $k$ ,

$$h_k^{(i+1)}(\mathbf{u}_{k\parallel}) = \frac{g_k(\mathbf{u}_{k\parallel})}{\int \rho_*(\mathbf{x}(\mathbf{u}_k)) \left( \prod_{j < k} h_j^{(i+1)}(\mathbf{u}_{j\parallel}(\mathbf{u}_k)) \right) \left( \prod_{j > k} h_j^{(i)}(\mathbf{u}_{j\parallel}(\mathbf{u}_k)) \right) d\mathbf{u}_{k\perp}}. \quad (12)$$

The iterations may be written in a more convenient and interpretable form by dividing Eq. (12) by  $h_k^{(i)}$ :

$$\frac{h_k^{(i+1)}(\mathbf{u}_{k\parallel})}{h_k^{(i)}(\mathbf{u}_{k\parallel})} = \frac{g_k(\mathbf{u}_{k\parallel})}{\int \rho_*(\mathbf{x}(\mathbf{u}_k)) \left( \prod_{j<k} h_j^{(i+1)}(\mathbf{u}_{j\parallel}(\mathbf{u}_k)) \right) \left( \prod_{j\geq k} h_j^{(i)}(\mathbf{u}_{j\parallel}(\mathbf{u}_k)) \right) d\mathbf{u}_{k\perp}}. \quad (13)$$

The  $h_k^{(i)}$  term in the denominator was absorbed by the integral using Eq. (9). Comparing to Eq. (8), we see that the denominator in Eq. (13) is the  $k$ th *simulated projection* of the MENT distribution function using the up-to-date component functions. Let us denote this projection  $\tilde{g}_k^\nabla(\mathbf{u}_{k\parallel})$  to indicate that the projection is computed during the inner loop. In this notation, Eq. (13) becomes

$$h_k^{(i+1)}(\mathbf{u}_{k\parallel}) = h_k^{(i)}(\mathbf{u}_{k\parallel}) \left( \frac{g_k(\mathbf{u}_{k\parallel})}{\tilde{g}_k^\nabla(\mathbf{u}_{k\parallel})} \right), \quad (14)$$

Finally, we add a learning rate, or damping coefficient,  $0 < \omega \leq 1$ , which slows the journey from the unconstrained to constrained maximum-entropy distribution [10]:

$$h_k^{(i+1)}(\mathbf{u}_{k\parallel}) = h_k^{(i)}(\mathbf{u}_{k\parallel}) \left( 1 + \omega \left( \frac{g_k(\mathbf{u}_{k\parallel})}{\tilde{g}_k^\nabla(\mathbf{u}_{k\parallel})} - 1 \right) \right). \quad (15)$$

(This may be necessary to avoid overfitting noisy data.) In summary, for each measurement index  $k$ , we divide the  $k$ th measurement by the  $k$ th simulated projection; then we repeat this loop until convergence.

#### IV. PARTICLE-BASED MENT

The iterations in Eq. (12) can be computed via numerical integration. Assume, for the moment, that each measurement has  $R^M$  pixels and that each transformed distribution is evaluated on a regular grid of size  $R^{(N-M)}$ . For each of the  $R^M$  bins, we must use the maps  $\mathcal{M}_k$  to transport all  $R^{(N-M)}$  integration points to each of the  $K$  measurement axes to evaluate the distribution function in Eq. (7). For a fixed integration grid, the computational cost is proportional to  $KR^M$ . Thus, integration-based solutions can become expensive when the phase space is high-dimensional or when there are many high-resolution measurements.

We suggest computing the projections by sampling particles from  $\rho(\mathbf{x})$  in Eq. (7), transporting the particles to the measurement locations, and binning them on the measurement axes. We refer to this strategy as particle-based MENT, compared to the conventional integration-based MENT solver. One could view the particle approach as a type of Monte Carlo integration. Two properties give particle-based MENT the ability to scale to larger problems. First, the computational cost scales

with  $K$ , rather than  $KR^M$  (binning particles on a one- or two-dimensional axis is very fast, regardless of the number of bins). Second, several strategies have been developed to sample from high-dimensional distributions. We describe two strategies in the following subsections.

(It may be worth noting that particle-based MENT does not require us to invert the phase space transformations and automatically enables non-symplectic transformations. (Integration-based MENT would require the determinant of the Jacobian of each transformation.) The only requirement on the transformations is that they are deterministic (so that there is a unique mapping between  $\mathbf{x}$  and  $\mathbf{u}_k$ ) and independent of the initial distribution. It is unclear if these features would ever be relevant in accelerator physics contexts, where the transformations are based on Hamiltonian dynamics.)

#### A. Grid Sampling (GS)

A simple and reliable sampling method is to evaluate the distribution on a grid, randomly select grid cells, and sample a particle from a uniform distribution over each cell. We call this Grid Sampling (GS):

1. Evaluate the probability density on a rectilinear grid, generating an  $N$ -dimensional image with  $C = R^N$  cells.
2. Flatten the image and compute the discrete probability distribution function  $f(\theta_i)$ , where  $\theta_i$  represents the cell number.
3. Compute the cumulative distribution function:

$$F(\theta_i) = \sum_{j<i} f(\theta_j). \quad (16)$$

4. Sample random numbers  $u$  from a uniform distribution on the unit interval  $[0, 1]$  and find the corresponding bins via the inverse transform:

$$\theta_i = F^{-1}(u). \quad (17)$$

5. Generate particle coordinates  $\mathbf{x}_i + \mathbf{\Delta}_i$ , where  $\mathbf{x}_i$  is the cell location in phase space and  $\mathbf{\Delta}_i$  is drawn from a uniform distribution over the cell volume.

With enough particles, GS reproduces the discretized version of the distribution. For smoothing, we may add

noise  $\epsilon \Delta_i$  to each particle, where  $\Delta_i$  is drawn from a uniform distribution over the particle's cell and  $\epsilon \geq 0$ . GS has no tuning parameters outside the smoothing parameter and grid resolution. By vectorizing the computations, the time complexity is (more or less) independent of the number of samples. Storing and transporting grids with  $C = R^4$  cells is not too problematic on personal computers when  $R \leq 40$ .  $R = 32$  bins are enough to represent most four-dimensional distributions of interest. If there are correlations between dimensions, we can boost the resolution along some dimensions by defining the sampling grid in “normalized” coordinates

$$\mathbf{z} = \mathbf{V}^{-1} \mathbf{x}. \quad (18)$$

If  $\mathbf{V}$  is chosen such that  $\langle \mathbf{z} \mathbf{z}^T \rangle = \mathbf{I}$ , the transformed grid will align with the distribution and the number of points overlapping the beam will be greater than if the grid was defined in the unnormalized space. Nonlinear transformations  $\mathbf{x} = \mathcal{V}(\mathbf{z})$  are also possible but have not been explored.

A six-dimensional version of grid sampling is possible, but only at low resolutions ( $R \approx 15$ ).

## B. Markov Chain Monte Carlo (MCMC)

Markov Chain Monte Carlo (MCMC) is a family of gridless sampling methods [11]. MCMC attempts to build a Markov chain—a sequence in which the next point depends only on the previous point—for which the equilibrium distribution is the target distribution. We focus on the Metropolis-Hastings (MH) sampling algorithm, one of the simplest MCMC variants [12]. MH explores the target distribution using a random walk, starting from point  $\mathbf{x}_0$ . Given the current point  $\mathbf{x}_t$ , MH proposes a new point  $\mathbf{x}_*$  drawn from the jumping distribution  $q(\mathbf{x}_*|\mathbf{x}_t)$ . Then, given a random number  $u$  drawn from a uniform distribution on the unit interval,  $\mathbf{x}_t$  is updated as

$$\mathbf{x}_{t+1} = \begin{cases} \mathbf{x}_* & \text{if } u \leq \pi(\mathbf{x}_*|\mathbf{x}_t), \\ \mathbf{x}_t & \text{otherwise,} \end{cases} \quad (19)$$

where

$$\pi(\mathbf{x}_*|\mathbf{x}_t) = \min \left( 1, \frac{\rho(\mathbf{x}_*) q(\mathbf{x}_t|\mathbf{x}_*)}{\rho(\mathbf{x}_t) q(\mathbf{x}_*|\mathbf{x}_t)} \right) \quad (20)$$

is the acceptance probability.

The Metropolis-Hastings algorithm has minimal computer storage requirements, does not need gradient or curvature information, and is guaranteed to converge to the target distribution  $\rho(\mathbf{x})$  in the long run. There is no guaranteed convergence rate; significant time can be spent in one mode of a multimodal distribution. Challenging distributions are typically very high-dimensional or highly irregular and, therefore (we hypothesize), unlikely to represent realistic beam distributions.

In typical MCMC applications, one only needs a few thousand samples to estimate the distribution's low-order moments or to compute expectation values under the distribution, usually in the context of Bayesian inference. In our application, we require many more samples to compute projected densities with high precision. To increase the sampling speed, we run multiple MCMC chains in parallel, each with a different starting point. In typical problems involving tens of measurements and linear phase space transformations, parallel sampling with hundreds of chains can generate one million samples in a few seconds. When using many parallel chains and running each chain for thousands of steps, we did not experience difficulties exploring multimodal distributions.

The Metropolis-Hastings algorithm performance depends on the jumping distribution. If the jumping distribution is too wide, the rejection rate will be too large. If the jumping distribution is too narrow, too much time will be spent in one part of the target distribution. A common choice is a Gaussian jumping distribution centered on the current point with a tunable covariance matrix.

## V. METHOD DEMONSTRATION

The remainder of this paper demonstrates particle-based MENT convergence in two numerical experiments. The first experiment uses GS sampling to fit a four-dimensional distribution to one-dimensional projections in a highly nonlinear system. The second experiment uses MCMC sampling to reconstruct a six-dimensional distribution from its 15 two-dimensional marginal projections. These experiments are not designed to reconstruct the true distribution. MENT generates the most conservative solution allowed by the constraints but does not guarantee the constraints are tight. Minimizing the reconstruction uncertainty is a question of experimental design and is beyond the scope of this paper. To assess the algorithm performance, we only need to compare the simulated projections to the measured projections.

In our first example, we consider four-dimensional phase space coordinates  $\mathbf{x} = (x, x', y, y')^T$  and a linear transformation of the form

$$\mathbf{M} = \begin{bmatrix} \cos \phi & \sin \phi & 0 & 0 \\ -\sin \phi & \cos \phi & 0 & 0 \\ 0 & 0 & \cos \phi & \sin \phi \\ 0 & 0 & -\sin \phi & \cos \phi \end{bmatrix}, \quad (21)$$

followed by an axially symmetric nonlinear map [13]:

$$\begin{bmatrix} x \\ x' \\ y \\ y' \end{bmatrix} \rightarrow \begin{bmatrix} x \\ x' \\ y \\ y' \end{bmatrix} + \begin{bmatrix} 0 \\ \delta \cos \theta \\ 0 \\ \delta \sin \theta \end{bmatrix}, \quad (22)$$

with  $x = r \cos \theta$ ,  $y = r \sin \theta$ , and

$$\delta(r) = -\frac{1}{2 \sin \phi} \left( \frac{r}{r^2 + 1} \right) - \frac{2r}{\tan \phi}. \quad (23)$$

The  $k$ th transformation  $\mathcal{M}_k$  is the combined action of the transfer matrix (Eq. (21)) followed by the nonlinear kick (Eq. (22)), repeated  $T_k$  times.

We chose an upright ( $\langle \mathbf{x}\mathbf{x}^T \rangle = \mathbf{I}$ ) initial distribution without cross-plane dependencies ( $\rho(x, x', y, y') = \rho(x, x')\rho(y, y')$ ), with hollow distributions in  $\rho(x, x')$  and  $\rho(y, y')$ . We generated training data for  $K = 4$  transformations with  $T_k = 15k$ , recording one-dimensional projections  $\{\rho(x), \rho(y)\}$  after each transformation, generating eight total profiles.

We used the Grid Sampling (GS) algorithm to sample particles from the four-dimensional MENT distribution. The sampling grid had resolution  $32^4$  and smoothing parameter  $\epsilon = 1$ . We ran MENT for three iterations with learning rate  $\omega = 0.95$  and  $2 \times 10^5$  sampled particles per iteration. Fig. 1 gives a sense of the reconstruction performance. The simulated profiles agree with the “measured” profiles. These profiles do not contain enough information to reconstruct the two-dimensional distributions plotted in the figure, which are hollow at the origin, although the main features are reproduced.

Extending MENT to six dimensions is motivated by the recent experiments in [14] and [15], which fit five- and six-dimensional distributions, respectively, to a set of two-dimensional beam profiles. In [14], the beamline consisted of upright quadrupoles followed by a polarizable transverse deflecting cavity, which indirectly measures the three-dimensional spatial distribution  $\rho(x, y, z)$ . In [15], the beamline consisted of upright quadrupoles, a transverse deflecting cavity, and a dipole bend [15]. The fit error in these experiments was small, and simulations seemed to indicate that the problem was well-constrained for a range of initial beams. Unlike the two-dimensional case, it is still unclear how to determine the ideal set of  $N$ -dimensional phase space transformations (without running the reconstruction algorithm for each option). Thus, it is unclear if these sets of optics are ideal, or whether they could be improved by varying their parameters or including other elements such as accelerating cavities, skew quadrupoles, solenoids, or nonlinear focusing elements.

Let us consider a more abstract problem. For a distribution without linear correlations between planes and a fixed number of measurements  $K = N(N - 1)/2$ , we hypothesize that the ideal set of measurements is the set of  $K$  two-dimensional marginals, i.e., pairwise projections. There are 15 pairwise projections of the six-dimensional phase space:  $\{\rho(x, x'), \rho(x, y), \rho(x, y'), \rho(x, z), \rho(x, z'), \rho(x', y), \rho(x', y'), \rho(x', z), \rho(x', z'), \rho(y, y'), \rho(y, z), \rho(y, z'), \rho(y', z), \rho(y', z'), \rho(z, z')\}$ . We will attempt to find the maximum-entropy distribution consistent with these projections. If the measurement axes are fixed, the phase space transformations needed to obtain these projections are permutation matrices. Equivalently, we may consider an identity transformation with multiple diagnostics measuring the different projections.

We used a Gaussian Mixture distribution as the ground

truth. The distribution is the superposition of seven Gaussian distributions, each with a random mean and variance. This distribution is highly irregular for beam physics applications, but it is a good candidate for initial model testing because it is multimodal, easy to sample from, and has clear structure when projected onto lower dimensions. We used the Metropolis-Hastings (MH) algorithm to sample particles from the six-dimensional MENT distribution. We used a Gaussian jumping distribution with covariance matrix  $0.1\hat{\Sigma}$  where  $\hat{\Sigma}$  is the covariance matrix of the target distribution. We simulated the projections on each iteration by running 500 parallel MCMC chains for 2000 steps to generate  $10^6$  total samples. The starting point of each chain was sampled from a Gaussian distribution with covariance matrix  $0.5\hat{\Sigma}$ .

The six-dimensional MENT algorithm converged in 1-2 epochs, each epoch taking less than 60 seconds. Fig. 2 plots the 15 pairwise projections from the trained MENT model and the true distribution. The simulated projections agree with the “measured” projections. Note that phase space distributions in accelerators are typically unimodal but may develop hollow structures as they evolve in nonlinear force fields [16]; this structure is more difficult to reconstruct from low-dimensional views [4, 17].

## VI. CONCLUSION

We have proposed an alternative implementation of the MENT algorithm that scales to high dimensional phase space. The method uses particle sampling, rather than numerical integration, to compute the distribution’s projections. The computational cost scales linearly with the number of measurements, but does not depend on the measurement resolution. We demonstrated that when the phase space dimension  $N \leq 4$ , an accurate grid-based sampler can be used with almost no hyperparameters to tune. We then showed that MCMC algorithms, such as the Metropolis-Hastings (MH) algorithm, can be used for higher-dimensional reconstructions. We used a parallel MH sampler to fit a six-dimensional distribution to 15 two-dimensional projections.

Investigation of four-dimensional integration-based MENT solvers should continue along with development of sample-based solvers. Six-dimensional MENT using MCMC appears promising, although further study is needed to refine the selection and tuning of the MCMC algorithm. A logical next step would be to test the algorithm on simulated data in diagnostic beamlines, then on real data. We have shared our MENT implementation in an open-source repository [18].

MENT, in its modern form, applies to a broad range of problems. The only requirements are that (i) the measurements are projections of the distribution, (ii) the transformations are deterministic, and (iii) the transformations do not depend on the initial distribution. Reconstructions with nonlinear transformations have not been

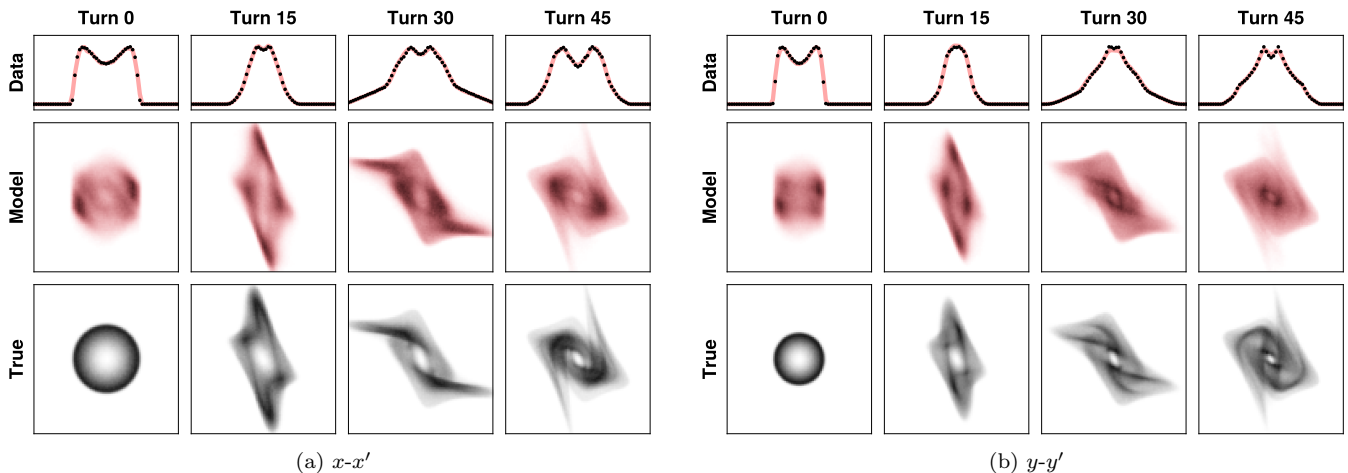


FIG. 1. Four-dimensional MENT reconstruction from  $x$  and  $y$  profiles on four different turns in a nonlinear periodic lattice. The top rows show the “measured” profiles (black) and simulated profiles (red). The bottom rows show the two-dimensional projections of the reconstructed four-dimensional distribution on each turn (red) compared to the true distribution (black).

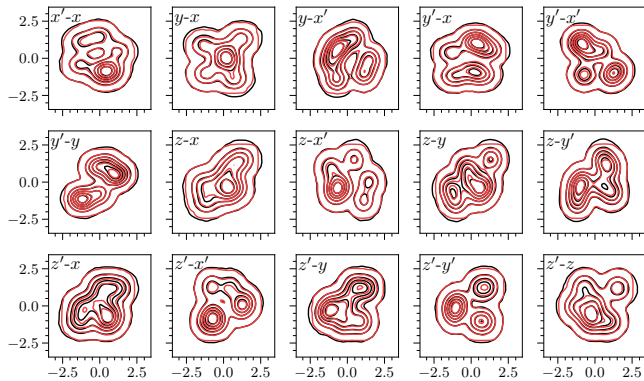


FIG. 2. Six-dimensional reconstruction of a Gaussian mixture distribution from two-dimensional marginal projections. Simulated projections are plotted in red, and true projections are plotted in black. Contours vary linearly from 1% to 100% of the peak density. Each plot shows a histogram of  $10^6$  samples drawn from the reconstructed distribution and binned on the two-dimensional axis. A Gaussian filter is applied to each image to reduce statistical noise from the binning process.

explored in depth, and it is unknown if nonlinearity expands or contracts the solution space; MENT could offer an efficient way to study this question. A particle-based MENT solver might also enable some type of iterative solution for beams with strong space charge, for which the transformations depend on the initial distribution. Finally, the MENT implementations discussed in this paper can generate an enormous number of samples, which

may enable high-dimensional reconstructions down to the noise level of the measurement devices.

Finally, MENT selects a single probability distribution  $\rho(\mathbf{x})$ —the most reasonable or probable distribution allowed by the constraints—and does not consider the reconstruction uncertainty. Consider a vector  $\boldsymbol{\theta}$  parameterizing the phase space distribution  $\rho_{\boldsymbol{\theta}}(\mathbf{x}) = \rho(\mathbf{x}|\boldsymbol{\theta})$ . The points  $\{\boldsymbol{\theta}\}$  compatible with the constraints form a *statistical manifold* with a unique metric [6, 19]. We are ultimately interested in a probability distribution over  $\boldsymbol{\theta}$ , conditional on the measured data. Evaluating the shape of this higher level distribution in the maximum-entropy framework is left as future work.

## VII. ACKNOWLEDGEMENTS

I thank J. C. Wong for fruitful discussions on maximum-entropy methods in phase space tomography. This manuscript has been authored by UT Battelle, LLC under Contract No. DE-AC05-00OR22725 with the U.S. Department of Energy. The United States Government retains and the publisher, by accepting the article for publication, acknowledges that the United States Government retains a non-exclusive, paid-up, irrevocable, world-wide license to publish or reproduce the published form of this manuscript, or allow others to do so, for United States Government purposes. The Department of Energy will provide public access to these results of federally sponsored research in accordance with the DOE Public Access Plan (<http://energy.gov/downloads/oe-public-access-plan>).

[1] C. McKee, P. O’Shea, and J. Madey, Phase space tomography of relativistic electron beams, Nuclear Instruments

and Methods in Physics Research Section A: Acceler-

- ators, Spectrometers, Detectors and Associated Equipment **358**, 264 (1995).
- [2] A. Wolski, D. C. Christie, B. L. Militsyn, D. J. Scott, and H. Kockelbergh, Transverse phase space characterization in an accelerator test facility, *Phys. Rev. Accel. Beams* **23**, 032804 (2020).
- [3] A. Wolski, M. A. Johnson, M. King, B. L. Militsyn, and P. H. Williams, Transverse phase space tomography in an accelerator test facility using image compression and machine learning, *Phys. Rev. Accel. Beams* **25**, 122803 (2022).
- [4] A. Hoover and J. C. Wong, High-dimensional maximum-entropy phase space tomography using normalizing flows, *Phys. Rev. Res.* **6**, 033163 (2024).
- [5] S. Pressé, K. Ghosh, J. Lee, and K. A. Dill, Principles of maximum entropy and maximum caliber in statistical physics, *Rev. Mod. Phys.* **85**, 1115 (2013).
- [6] A. Caticha, Entropy, information, and the updating of probabilities, *Entropy* **23**, 895 (2021).
- [7] G. Minerbo, MENT: A maximum entropy algorithm for reconstructing a source from projection data, *Computer Graphics and Image Processing* **10**, 48 (1979).
- [8] G. N. Minerbo, O. R. Sander, and R. A. Jameson, Four-dimensional beam tomography, *IEEE Transactions on Nuclear Science* **28**, 2231 (1981).
- [9] J. C. Wong, A. Shishlo, A. Aleksandrov, Y. Liu, and C. Long, 4D transverse phase space tomography of an operational hydrogen ion beam via noninvasive 2d measurements using laser wires, *Physical Review Accelerators and Beams* **25**, 10.1103/PhysRevAccelBeams.25.042801 (2022).
- [10] C. Mottershead, Maximum entropy tomography, in *Proceedings of the Fifteenth International Workshop on Maximum Entropy and Bayesian Methods, Santa Fe, New Mexico, USA* (Springer, 1996) pp. 425–430.
- [11] A. Gelman, J. B. Carlin, H. S. Stern, and D. B. Rubin, *Bayesian data analysis* (Chapman and Hall/CRC, 1995).
- [12] N. Metropolis, A. W. Rosenbluth, M. N. Rosenbluth, A. H. Teller, and E. Teller, Equation of state calculations by fast computing machines, *The journal of chemical physics* **21**, 1087 (1953).
- [13] T. Zolkin, B. Cathey, and S. Nagaitsev, Dynamics of mcmillan mappings ii. axially symmetric map, arXiv preprint arXiv:2405.05657 (2024).
- [14] S. Jaster-Merz, R. W. Assmann, R. Brinkmann, F. Burkart, W. Hillert, M. Stanitzki, and T. Vinatier, 5D tomographic phase-space reconstruction of particle bunches, *Phys. Rev. Accel. Beams* **27**, 072801 (2024).
- [15] R. Roussel, J. P. Gonzalez-Aguilera, A. Edelen, E. Wisniewski, A. Ody, W. Liu, Y.-K. Kim, and J. Power, Efficient 6-dimensional phase space reconstruction from experimental measurements using generative machine learning (2024).
- [16] K. Ruisard, A. Aleksandrov, S. Cousineau, V. Tzoganis, and A. Zhukov, High dimensional characterization of the longitudinal phase space formed in a radio frequency quadrupole, *Phys. Rev. Accel. Beams* **23**, 124201 (2020).
- [17] A. Hoover, K. Ruisard, A. Aleksandrov, A. Zhukov, and S. Cousineau, Analysis of a hadron beam in five-dimensional phase space, *Phys. Rev. Accel. Beams* **26**, 064202 (2023).
- [18] <https://github.com/austin-hoover/ment>.
- [19] A. Caticha and R. Preuss, Maximum entropy and bayesian data analysis: Entropic prior distributions, *Phys. Rev. E* **70**, 046127 (2004).